WOOD RESEARCH doi.org/10.37763/wr.1336-4561/71.1.3852
e-ISSN 2729-8906
71(1): 2026 38-52 pp.

CORE-SHELL AG-TIO$_2$@EVA PREPARATION AND ITS APPLICATION IN WOOD ANTI-FUNGAL, ANTI-MOLD AND ANTI-DECAY RESEARCH

TING LIU, YAOXING SUN, HONGGANG ZHAO, HUACHUN QI, JIUYIN PANG
BEIHUA UNIVERSITY
CHINA

(RECEIVED OCTOBER 2025)

ABSTRACT

Using silver-loaded nano-TiO_2 (Ag-TiO_2) and ethylene-vinyl acetate (EVA) emulsion as raw materials, a core-shell structured Ag-TiO_2@EVA composite material was synthesized to impart antimicrobial, mold-proof, and decay-resistant properties to wood. The study investigated the composite material's efficacy in controlling wood-staining fungi and molds, as well as its decay resistance and antifungal performance. The results showed that when the film thickness was between 0.12 to 0.15 mm with an Ag-TiO_2 content of 20% or more, or when the film thickness was between 0.21 to 0.24 mm with an Ag-TiO_2 content of 15% or more, the control efficacy against *Botryodiplodia theobromae* and *Aspergillus niger* reached 100%, and the decay resistance grade against *Poria placenta* was level I. For samples with 10% Ag-TiO_2 content, the inhibition zone diameters against *A. niger* and *B. theobromae* were both greater than 10 mm, while samples with 15% and 20% Ag-TiO_2 content exhibited inhibition zones larger than 20 mm, indicating strong antimicrobial effects.

KEYWORDS: Core-shell structure, wood anti-mold, antifungal, EVA.

INTRODUCTION

Wood, as a renewable natural biomaterial, is widely utilized in construction, furniture, and decorative applications (He et al. 2021; Jian et al. 2022; Chen et al. 2022). However, its susceptibility to microbial degradation leads to decay, mold growth, and discoloration, significantly compromising its functional value and aesthetics (Zhang et al. 2016; Selim et al. 2017; Teng et al. 2018; Emmerich et al. 2021). To address these issues, researchers have dedicated efforts to developing effective wood preservation technologies. Surface treatments, such as applying chemical preservatives, are common industrial practices. Preservatives such as chromated copper arsenate (CCA), pentachlorophenol, and copper naphthenate are widely used for their antimicrobial properties. However, these chemicals contain toxic components such as arsenic and chromium, posing risks to human health and the environment (Cao 2006;

Yang 2011; Xi and Jiang 2013; Sun et al. 2017; Rockwood et al. 2022). Traditional organic compounds as preservatives have certain drawbacks, leading researchers to focus on the efficacy of inorganic metals as wood preservatives. The use of inorganic metals and metal oxides as antimicrobial agents is already widespread, with metals such as Ag, Au, and TiO_2 being the most common and extensively applied metal-based antimicrobial materials (Zhao et al. 2012; Shams et al. 2019; Cui et al. 2012; Jin et al. 2014; Li et al. 2020; Persaud et al. 2020). Notably, Ag and TiO_2 are particularly favoured. Gunputh et al. (2020) and Mohandas et al. (2017) combined Ag and TiO_2 by layering Ag on TiO_2 surfaces, thereby achieving effective bactericidal effects against *Escherichia coli* and *Staphylococcus aureus*.

However, conventional inorganic metal antimicrobial agents alone cannot meet the requirements for long-lasting sterilization, and common wood preservatives also fail to ensure sustained anti-decay efficacy. To address this challenge, this study employs a core-shell structure. The core-shell structure refers to a composite material where one material serves as the core, and single or multiple shell layers are designed around it (Lu et al. 2024; Gao et al. 2021; Choi et al. 2018). These attributes make core-shell structures highly suitable for controlled release systems, sterilization, and preservation applications (Chuang et al. 2023; Lei et al. 2023). To achieve prolonged antibacterial effects by delaying the release of Ag-TiO_2 and improving antimicrobial performance, this study utilizes ethylene-vinyl acetate (EVA) copolymer as the outer shell material to encapsulate Ag-TiO_2, forming a core-shell structure. EVA, a widely used polymer, is selected as the carrier material for Ag-TiO_2 due to its excellent film-forming ability and mechanical properties. Borreguero et al. (2011) prepared low-density polyethylene/EVA -embedded wax phase-change microcapsules via spray drying, achieving a microencapsulation efficiency of 63%. The resulting microcapsules exhibited superior mechanical performance and phase-change cycling stability (up to 3000 cycles), matching the heat storage capacity of commercial polystyrene phase-change microcapsules. Zhou et al. (2023) removed the solvent to prepare core-shell particles with SiO_2 as the core and maleic anhydride-grafted ethylene-vinyl acetate copolymer (EVA-g-MAH) as the shell. By adjusting the feed ratio of SiO_2 to EVA-g-MAH, the thickness of the rubber shell could be precisely controlled.

This study employed a straightforward post-emulsification method to synthesize Ag-TiO_2@EVA core-shell composite materials. These composites were applied to wood surfaces to form antibacterial films, aiming to enhance wood protection against fungi and molds by improving antibacterial, anti-mold, anti-discoloration, and decay-resistant performance. The research seeks to develop a novel wood anti-mold agent that meets current industry standards-non-toxic, environmentally benign, and offering long-term efficacy.

MATERIAL AND METHODS

Material

Poplar (*Populus ussuriensis* Kon.) specimens were collected from Sanhe Forest Farm, Jiaohe Forestry Experimental Bureau, Jilin Province. Sapwood sections with straight grain, no decay/discoloration, and uniform texture were processed along the longitudinal axis (density: 0.440 g/cm³; moisture content: 12%) into 50 mm (L) × 20 mm (W) × 5 mm (T) blocks for wood

anti-mold testing (n=192). All specimens were oven-dried at 103℃ to absolute dryness before testing. Larch (*Larix gmelinii* (Rupr.) Kuzen.) specimens from the same provenance were similarly processed (density: 0.62 g/cm³; moisture content: 15%) into 20 mm (L) × 20 mm (W) × 20 mm (T) cubes for wood decay resistance testing (n=288) and identically dried.

Chemicals: Ethylene-vinyl acetate (EVA) emulsion (industrial grade, Dalian Chem, Jiangsu Co., Ltd.); silver-loaded nano-TiO_2 (designation: VK-T07; Ag content: 3% w/w, Hangzhou Tuoming New Material Co., Ltd.); dichloromethane (analytical grade); Tween 80 (analytical grade). Molds included *Aspergillus niger, Botryodiplodia theobromae* Pat., and *Poria placenta* were sourced from China Center for Type Culture Collection - Forestry Division.

Methods

Preparation of Ag-TiO_2@EVA emulsion

Dissolve a measured quantity of EVA emulsion in dichloromethane at 50℃, followed by stirring in Ag-TiO_2 and ultrasonicating the mixture for 30 min to disperse Ag-TiO_2 uniformly in the EVA/dichloromethane solution. React this solution at 50℃ for 24 h to form a mixed suspension of Ag-TiO_2, EVA and dichloromethane. Add the prepared suspension to an aqueous emulsifier solution containing Tween 80, then emulsify the mixture at 10000 rpm for 2 min to generate an Ag-TiO_2/EVA/ dichloromethane-water emulsion. Subject the emulsion to mechanical stirring at 50℃ for 12 h to completely volatilize dichloromethane, leaving an Ag-TiO_2@EVA/ water emulsion. After cooling and removing excess water, collect the final product. Three variants of Ag-TiO_2@EVA core-shell structured emulsions were prepared with Ag-TiO_2 to EVA content at 10%, 15% and 20%.

Transmission electron microscopy (TEM) characterization

The 70-fold diluted Ag-TiO_2@EVA emulsion was directly deposited onto a copper grid and dried at room temperature to prepare observation specimens. These specimens were examined using a transmission electron microscope (TEM) (Tecnai G² 20, FEI Company, Netherlands) operated at an accelerating voltage of 200 kV.

Fourier transform infrared spectroscopy (FTIR) analysis

The dried samples were analysed using a Fourier transform infrared (FTIR) spectrometer (IRAffinity-1s, Shimadzu Corporation) at room temperature. A 2 g sample was dried in an electric thermostatic blower dryer at 120℃ for 4 h, followed by FTIR measurement in the range of 400 to 4000 cm^{-1} with a resolution of 2 cm^{-1} and 64 accumulations.

Emulsion stability testing

An aliquot of the test emulsion was placed in a centrifuge tube and vertically stored for 48 h at ambient temperature to test storage stability. The emulsion was considered unstable if sedimentation, flocculation, or delamination was observed; otherwise, it was deemed stable. An aliquot of the test emulsion in a centrifuge tube was symmetrically positioned in the rotor sockets, ensuring balanced tube mass distribution. Centrifugation was performed at 3000 rpm

for 10 min. Following centrifugation, the emulsion was evaluated for stability: homogeneous appearance indicated stability, while sedimentation or delamination denoted instability.

Antibacterial testing

The antibacterial performance of emulsions was evaluated using the filter paper disk method. Paper disks (5 mm diameter) impregnated with emulsion samples were placed on agar plates pre-inoculated with test bacteria. Plates were incubated at 25℃ ± 2℃ for 72 h. The presence of inhibition zones around disks was observed, and zone diameters were measured. According to GB/T 20944.1: 2007, results were classified as follows: no antibacterial effect (≤7 mm), weak antibacterial activity (≤10 mm), moderate activity (10 to 20 mm), or strong activity (≥20 mm). Three parallel tests were performed per sample.

Mold resistance determination

Preparation of poplar mold-resistant specimens

The Ag-TiO_2@EVA micro-composite material emulsion was uniformly coated on all six surfaces of Daqingyang poplar specimens, fully encapsulating them. Four film thicknesses were prepared: 0.12 to 0.15 mm, 0.15 to 0.18 mm, 0.18 to 0.21 mm, and 0.21 to 0.24 mm. For each thickness and sample type, 12 specimens were prepared: 6 specimens inoculated with *Aspergillus niger*, 6 specimens inoculated with *Botryodiplodia theobromae*. Control specimens (12 per thickness, 6 for each fungus) were also prepared. Each group underwent three independent replicate experiments, resulting in a total of 192 specimens.

After inoculation, both mold-resistant and control specimens were placed in a constant temperature and humidity chamber at 25 ± 2℃ and 75% relative humidity for fungal infection. Mold resistance was evaluated after 4 weeks. Following GB/T 18261 (2013), the infected specimens were graded into 5 levels based on infection area and characteristics, with infection values serving as quantitative indicators.

Tab. 1: Discoloration and grading of specimens after bacterial infection.

Infection value	Area of infection of the specimen.
0	No visible hyphae or mold spots on the specimen surface.
1	Infected area < 1/4 of the specimen surface.
2	Infected area between 1/4 to 1/2 of the specimen surface.
3	Infected area between 1/2 to 3/4 of the specimen surface.
4	Infected area > 3/4 of the specimen surface.

According to the infection value in Tab. 1, the control efficiency can be calculated, which can be used to evaluate the anti-mold and anti-discoloration ability of the antifungal agent. The higher prevention efficacy value indicated a stronger ability, as determined by Eq. 1:

$$E = (1 - \frac{D_1}{D_0}) \times 100\% \quad (1)$$

where: E is prevention efficacy (%), D_1 is infection value of antifungal-coated specimens, and D_0 is infection value of control specimens.

Wood anti-decay testing

Preparation of larch anti-decay specimens

Ag-TiO_2@EVA emulsion was uniformly coated on all six surfaces of larch specimens to achieve complete encapsulation. Four film thickness ranges were applied: 0.12 to 0.15 mm, 0.15 to 0.18 mm, 0.18 to 0.21 mm, and 0.21 to 0.24 mm. For each thickness, three specimens were dried to constant weight in an oven at (103±2)℃, followed by mass measurement. These specimens were then placed in culture bottles inoculated with *Poria placenta.* A blank control group was established, and three replicates per group were performed, totalling 144 specimens.

Fungal decay of preservative-treated specimens

After placing the culture bottles containing preservative-treated specimens into a constant temperature and humidity chamber at 25℃±2℃ and 75% relative humidity, they were incubated for 12 weeks. Following incubation, specimens were removed, and surface mycelia and impurities were gently scraped off. Each specimen was then dried to constant weight in an oven at (103±2)℃, individually weighed, and its mass loss rate calculated to evaluate the wood's natural decay resistance grade according to standard criteria. The mass loss rate (L) for each specimen was calculated as a percentage using Eq. 2:

$$L = (1 - \frac{W_1}{W_2}) \times 100\% \quad (2)$$

where: L - mass loss rate (%), W_1 - oven-dry mass of the specimen before testing (g), W_2 - oven-dry mass of the specimen after testing (g).

Decay resistance rating evaluation

According to GB/T 13942.1-2009, specimens are classified into five decay resistance grades based on mass loss rate (%) after a 12-week fungal decay test.

RESULTS AND DISCUSSION

Ag-TiO_2@EVA emulsion stability

The stability of emulsions is a critical indicator for evaluating their performance. As shown in Fig.1, the Ag-TiO_2@EVA emulsion exhibits excellent stability, maintaining homogeneity over long-term storage with no delamination or sedimentation. This indicates that varying Ag-TiO_2 loading consistently yielded stable emulsions. Typically, inorganic particles disperse poorly in organic matrices and tend to agglomerate and sediment, compromising polymer stability. However, physical encapsulation by organic polymers significantly mitigates this agglomeration. Tab. 3 further confirms the emulsion's stability: Storage stability: No phase separation after prolonged standing. Centrifugal stability: No sedimentation or delamination after centrifugation (3000 rpm, 10 min). These results demonstrate that most Ag-TiO_2 particles are effectively encapsulated by EVA, forming a core-shell structure.

Tab. 3: Effect of Ag-TiO_2 loading on emulsion stability and particle size.

Ag-TiO_2 addition /%	Storage stability	Centrifugal stability
10	stability	stability
15	stability	stability
20	stability	stability

FT-IR structural characterization of Ag-TiO_2@EVA

Fig. 2 shows the FT-IR spectra of EVA, Ag-TiO_2, and Ag-TiO_2@EVA. From the absorption peaks at 1740 cm^{-1}, 2900 cm^{-1}, 1240 cm^{-1}, and 1020 cm^{-1} correspond to the C=O stretching vibration, C-H stretching vibration, and C-O stretching vibrations in EVA, respectively. From Fig. 3b, the peak at 566 cm^{-1} is attributed to the Ti-O-Ti vibration, while the peaks at 3415 cm^{-1} and 1644 cm^{-1} correspond to the stretching and bending vibrations of -OH groups. In Fig. 3c, the Ag-TiO_2@EVA spectrum retains all major characteristic peaks of EVA, confirming that the addition of Ag-TiO_2 does not disrupt the backbone structure of EVA. However, compared to pure EVA, the Ag-TiO_2@EVA spectrum exhibits an additional Ti-O-Ti absorption peak at 566 cm^{-1}, indicating successful physical encapsulation of Ag-TiO_2 by EVA. The absence of new chemical bonds and the persistence of Ag-TiO_2's characteristic peak in the composite suggest that the interaction is predominantly physical, with the inorganic structure remaining intact. Thus, Ag-TiO_2 incorporation preserves EVA's chemical structure while modifying its physical properties, particularly in film-forming applications.

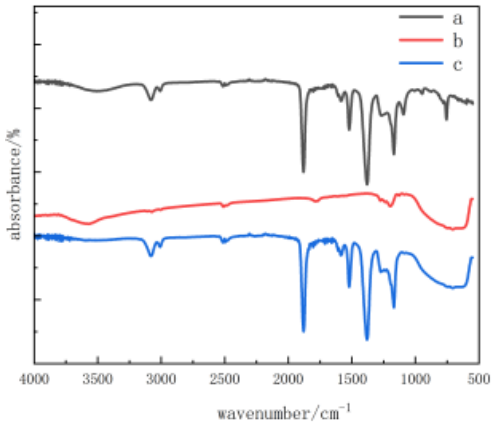

Fig. 2: FT-IR spectra of Ag-TiO_2@EVA composites:(a) EVA ;(b) Ag-TiO_2 ;(c) Ag-TiO_2@EVA.

Microstructural characterization of Ag-TiO_2@EVA

As shown in Fig. 3, which presents the TEM image of Ag-TiO_2@EVA, the composite exhibits a distinct core-shell structure with an overall spherical morphology. The average particle size is approximately 70 nm, consisting of a core measuring about 60 nm and a shell layer of around 10 nm. TEM observations reveal that despite variations in the core-shell ratio, the shell thickness of the three Ag-TiO_2@EVA composites remains around 10 nm. However, the sample with 20% Ag-TiO_2 loading shows a slightly thicker shell, reaching up to 13 nm. This phenomenon can be attributed to the fixed core size (60 nm for Ag-TiO_2). According to adsorption theory, the amount of adsorbate on particle surfaces is proportional to the surface area of the core particles. Therefore, differences in the core-shell ratio have minimal impact on the overall particle size.

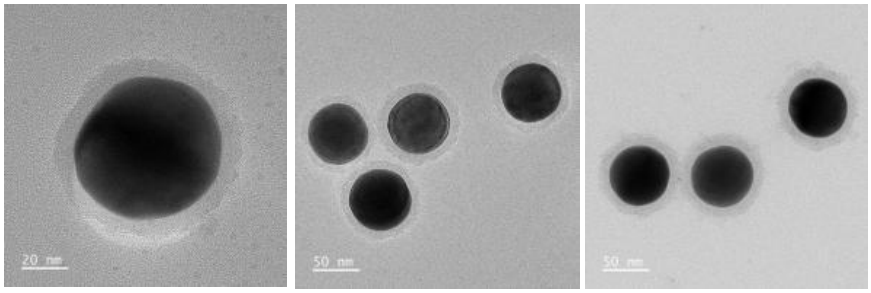

(a) (b) (c)

Fig. 3: TEM photographs of Ag-TiO_2@EVA (a) 10%;(b) 15%;(c)20%.

Antifungal properties of Ag-TiO_2@EVA

As shown in Tab. 4, antifungal efficacy improves with increasing Ag-TiO_2 loading, evidenced by larger inhibition zone diameters. The inhibition zones against *Aspergillus niger* exceed those against *Botryodiplodia theobromae*, indicating stronger suppression of *A. niger*. At 0% loading, no inhibition zones appear for either fungus, confirming EVA lacks antifungal activity. With 10% Ag-TiO_2, inhibition zones exceed 10 mm for both fungi, demonstrating moderate antifungal activity. At 15% and 20% loading, zones for *A. niger* measure 24.67 mm and 28.52 mm, while for *B. theobromae* reach 22.14 mm and 27.41 mm, all surpassing 20 mm and indicating strong antifungal activity.

Tab.4: Effect of Ag-TiO_2 loading on antifungal performance.

Ag-TiO_2 addition/%	Inhibition zone diameter/mm	
	Botryodiplodia theobromae	*Aspergillus niger*
0%	0	0
10%	16.81	17.76
15%	22.14	24.67
20%	27.41	28.52

Fig. 4 reveals circular inhibition zones for *A. niger* but irregular zones for *B. theobromae*. This distinction arises from their reproductive strategies: *A. niger* relies on rapid sporulation, and Ag-TiO_2@EVA inhibits spore germination within the zone, halting growth at its periphery. Conversely, *B. theobromae* exhibits slow sporulation (~2 months) but aggressive hyphal expansion. Hyphae partially overgrow the inhibition zone, causing irregularity despite clear antifungal efficacy.

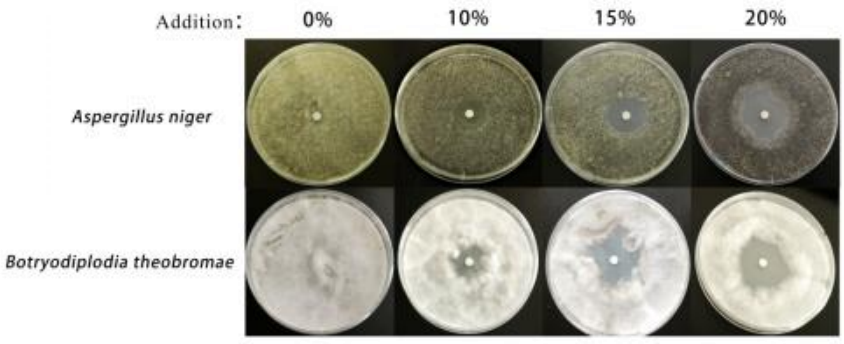

Fig. 4: Antifungal effect diagram of Ag-TiO_2@EVA emulsion.

Efficacy of Ag-TiO_2@EVA films against *Botryodiplodia theobromae*

As shown in Tab. 5, an increase in film thickness enhances the control efficacy. When the Ag-TiO_2 addition is 0%, and the film thickness increases from 0.12 to 0.15 mm to 0.21 to 0.24 mm, the infection value decreases from 3.7 to 2.3, while the control efficacy rises from 9% to 42%. This indicates that a thicker film improves protective performance, suggesting that the dense physical barrier formed by the pure EVA film provides a certain, albeit limited, degree of protection to the wood. This finding is consistent with the conclusions of Han research (Han et al. 2023). When the film thickness is maintained at 0.12 to 0.15 mm and the Ag-TiO_2 addition reaches 10%, the infection value drops to 1.8, with a control efficacy of 56%. At a 20% Ag-TiO_2 addition, the infection value becomes 0, achieving 100% control efficacy. This demonstrates that, under constant film thickness, increasing the Ag-TiO_2 content effectively prevents wood infection by *Botryodiplodia theobromae*, which can be attributed to the intrinsic antifungal properties of Ag-TiO_2 that inhibit fungal growth. As previously indicated (Tab. 4), a 20% Ag-TiO_2 addition exhibits superior antifungal efficacy compared to 10% or 15% additions, resulting in higher control efficacy.

B. theobromae wood through hyphal growth within surface and internal wood pores. Fig. 6a shows that untreated wood samples are heavily penetrated by thick, robust, and densely distributed hyphae after infection (indicated by yellow arrows). Compared to the untreated sample, the control sample (with EVA but without antimicrobial agents) exhibits a slight reduction in hyphae, but they still extensively occupy the cell cavities. This observation corresponds to the infection value reported in Tab. 5, indicating limited protective effect of the EVA film alone (Fig. 6b). When the Ag-TiO_2 addition is 15%, only a small amount of thin, poorly developed hyphae is observed inside the wood cells (Fig. 6c), demonstrating strong antifungal activity of the Ag-TiO_2@EVA composite and enhanced wood protection. At 20% Ag-TiO_2, no hyphal growth is detected (Fig. 6d), confirming excellent antimicrobial efficacy and complete inhibition of *B. theobromae*

Tab. 5: Effect of Ag-TiO_2 loading and film thickness on control efficacy against Botryodiplodia theobromae.

Film thickness/mm	Mass fraction of Ag-TiO_2/%	Infection value	Prevention and control efficacy/%
0	0	4	0
0.12~0.15	0	3.7	9
	10	1.8	56
	15	1	75
	20	0	100
0.15~0.18	0	3.3	18
	10	1.5	64
	15	0.8	80
	20	0	100
0.18~0.21	0	2.8	30
	10	1.3	68
	15	0.3	88
	20	0	100
0.21~0.24	0	2.3	43
	10	0.7	84
	15	0	100
	20	0	100

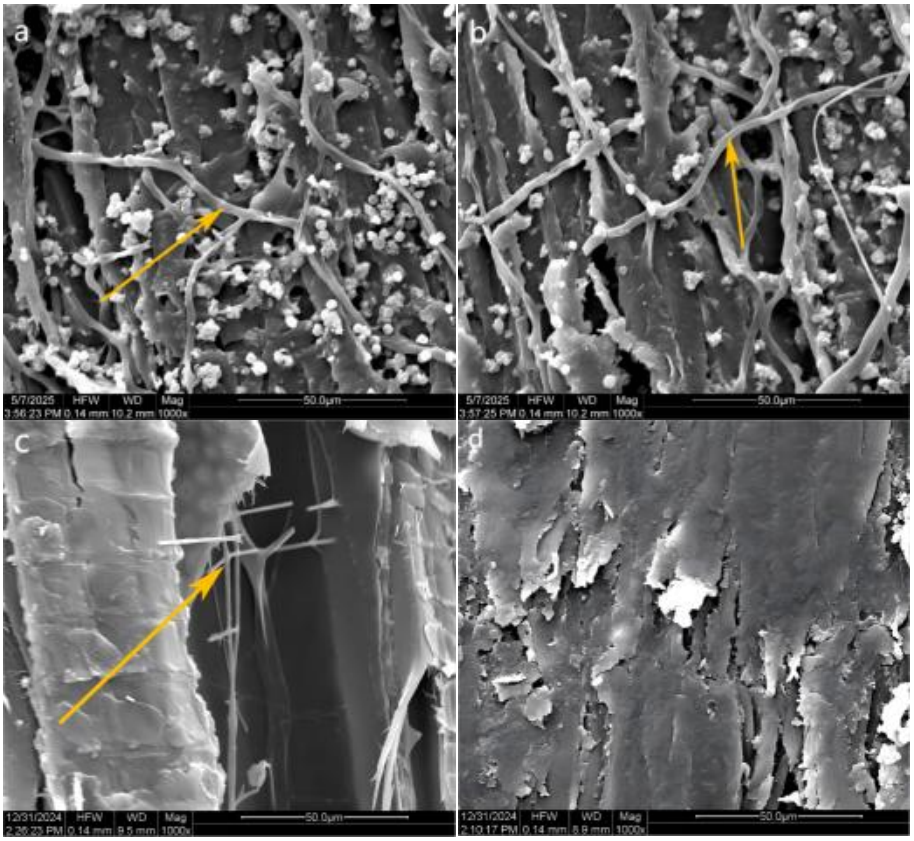

Fig. 5: SEM image of wood samples eroded by Botryodiplodia theobromae: (a) materials;(b) 0% control material (c)15% additive-treated material;(d)20% additive-treated material.

Efficacy of Ag-TiO_2@EVA films against *Aspergillus niger*

Tab. 6 indicates that, similar to the trend observed with *Botryodiplodia theobromae*, the control efficacy of the EVA emulsion against *Aspergillus niger* with film thickness even without Ag-TiO_2 addition, though the effect remains limited. At a film thickness of 0.12 to 0.15 mm and 0% Ag-TiO_2, the infection value is 3.5 with a control efficacy of only 13%. This infection value is 0.2 lower than that for *B. theobromae*, suggesting that *A. niger* a weaker ability to penetrate the EVA film, likely due to its primary reliance on spore reproduction compared to the hyphal penetration strategy of *B. theobromae*. Adding 10% Ag-TiO_2 reduces the infection value to 1.3 and increases control efficacy to 68%. At 20% Ag-TiO_2, the infection value drops to 0, achieving 100% efficacy. This demonstrates the superior effectiveness of the Ag-TiO_2@EVA composite against *A. niger*, effectively preventing wood infection. These findings are consistent with research by Zhang et al. (2016), confirming the significant inhibitory effect of Ag-TiO_2 on *A. niger* even at low concentrations.

Fig.7a shows untreated wood samples heavily infected with numerous spores of *A. niger*. Compared to the untreated sample, the control (EVA without antimicrobial agents) exhibits a slight reduction in hyphae and spores, but they remain plump and well-developed, indicating limited protective efficacy (Fig. 7b). With 15% Ag-TiO_2 (Fig. 7c), hyphal and sporular growth are significantly reduced and appear flattened, demonstrating the composite's ability to inhibit spore germination. At 20% Ag-TiO_2 (Fig. 7d), no hyphal or spore growth is observed, confirming optimal antifungal performance.

Tab. 6: Effect of Ag-TiO_2 loading and film thickness on control efficacy against Aspergillus niger.

Film thickness/mm	Mass fraction of Ag-TiO_2/%	Infection value	Prevention and control efficacy/%
0	0	4	0
0.12~0.15	0	3.5	13
	10	1.3	68
	15	0.7	82
	20	0	100
0.15~0.18	0	3.3	18
	10	1	75
	15	0.2	95
	20	0	100
0.18~0.21	0	2.7	33
	10	0.8	79
	15	0	100
	20	0	100
0.21~0.24	0	2.2	45
	10	0.5	88
	15	0	100
	20	0	100

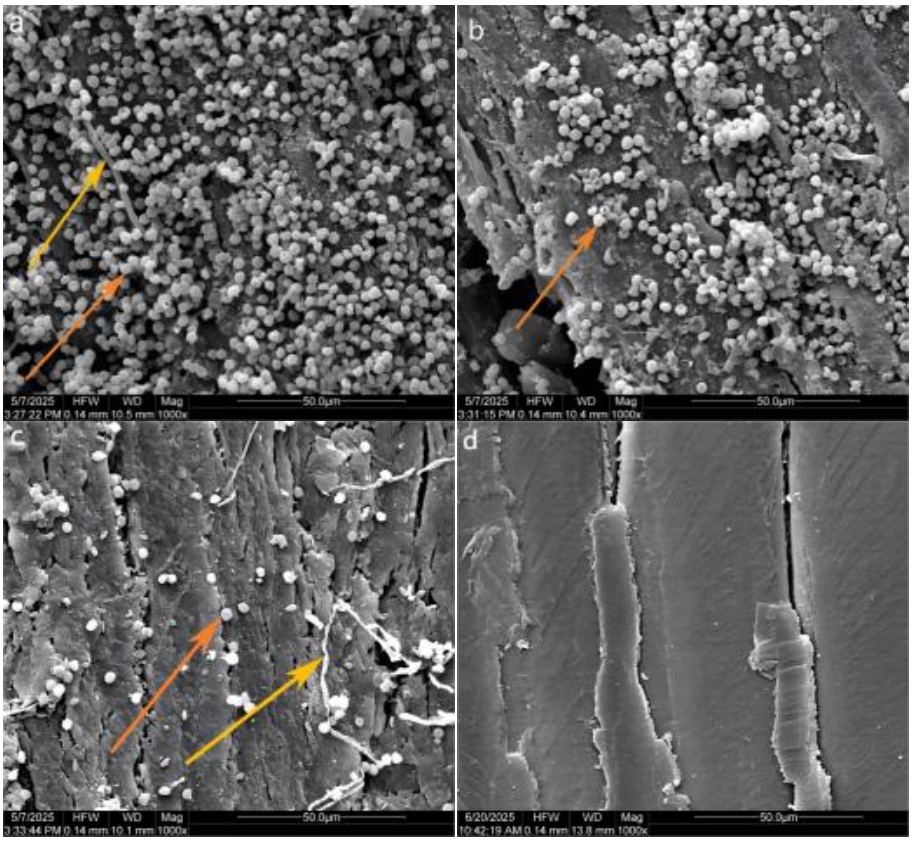

Fig. 6: SEM image of wood sample after Aspergillus niger attack: (a) materials; (b) 0% control material;(c) 15% additive-treated material;(d) 20% additive-treated material.

Wood decay resistance of Ag-TiO_2@EVA films

Tab. 7 shows that the mass loss rate of treated samples gradually decreased with increasing film thickness and Ag-TiO_2 addition. At a film thickness of 0.12 to 0.15 mm and 10% Ag-TiO_2, the decay resistance reached Grade II, with a mass loss rate of 19.19%, representing

a significant reduction compared to the 0% addition. When the Ag-TiO_2 addition was 20% at the same thickness, or 15% at a higher thickness of 0.18 to 0.21 mm, the decay resistance improved to Grade I. These results demonstrate that the inhibitory effect of Ag-TiO_2 against *Poria placenta* strengthens with higher additive concentrations, providing effective wood preservation. In contrast, alternative preservatives, such as the ginkgo heartwood chloroform extract used by Zhang et al. (2025) and *Trichoderma viride* NY45 employed by Jiang et al. (2025), required substantially higher concentrations to achieve Grade I efficacy, indicating the superior performance of metal-based Ag-TiO_2.

Tab. 7: Effects of film-forming thickness and Ag-TiO_2 mass fraction on the control efficacy of Poria placenta.

Film thickness/mm	Mass fraction of Ag-TiO_2/%	Mass loss rate/%	Corrosion resistance grade
0	0	62.71	IV
0.12~0.15	0	41.18	III
	10	19.19	II
	15	16.32	II
	20	10.78	I
0.15~0.18	0	36.48	III
	10	15.46	II
	15	12.68	II
	20	7.96	I
0.18~0.21	0	33.72	III
	10	10.80	II
	15	7.16	I
	20	4.43	I
0.21~0.24	0	30.58	III
	10	7.84	II
	15	5.96	I
	20	2.68	I

SEM images in Fig. 8 provide morphological evidence: the untreated wood (Fig. 8a) showed extensive hyphal growth of *Poria placenta*. The control sample (with EVA only, Fig. 8b) exhibited a reduction in hyphae compared to the untreated wood. In the sample with 15% Ag-TiO_2 (Fig. 8c), hyphal growth was significantly suppressed. Notably, with 20% Ag-TiO_2 (Fig. 8d), the wood surface appeared clean and well-preserved, with only minimal hyphae attached to the inner cell walls, indicating strong inhibition of fungal growth. The SEM observations are consistent with the mass loss data, confirming the efficacy of the Ag-TiO_2@EVA composite.

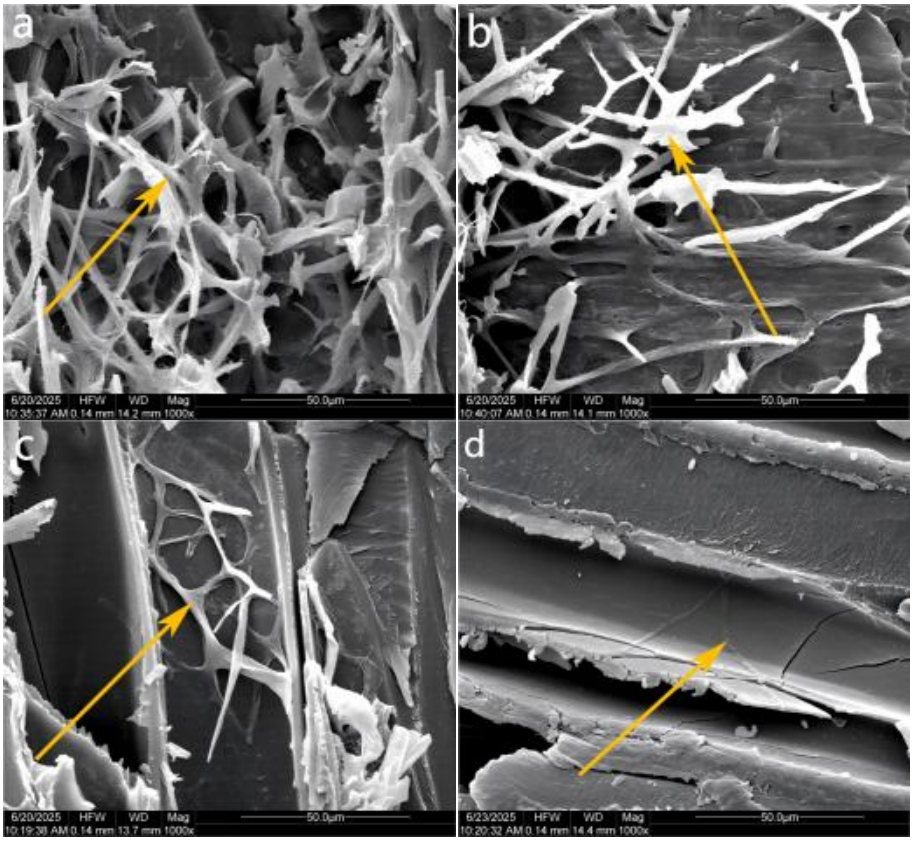

Fig. 7: SEM image of wood sample after Poria placenta attack: (a)materials; (b) 0% control material;(c) 15% additive-treated material;(d) 20% additive-treated material.

CONCLUSIONS

(1) Core-shell Ag-TiO_2@EVA composites were synthesized using Ag-TiO_2 as the core and EVA emulsion as the shell, exhibiting distinct spherical morphology with smooth surfaces and an average particle size 70 nm. *(2)* Antifungal efficacy against *Aspergillus niger* and *Botryodiplodia theobromae* improved with increasing Ag-TiO_2 loading. At 15% and 20% loading, inhibition zones reached 24.67 mm (*A. niger*, 15%), 28.52 mm (*A. niger*, 20%), 22.14 mm (*B. theobromae*, 15%), and 27.41 mm (*B. theobromae*, 20%), demonstrating strong antimicrobial activity. *(3)* With increasing Ag-TiO_2 loading, the control efficacy of Ag-TiO_2@EVA composites against *Aspergillus niger* and *Botryodiplodia theobromae* improves, while the decay resistance grade against *Poria placenta* elevates. 100% control efficacy against *A. niger* and *B. theobromae* is achieved under either of the following conditions: Film thickness: 0.12 to 0.15 mm + Ag-TiO_2 loading ≥20%, or Film thickness: 0.21 to 0.24 mm, Ag-TiO_2 loading ≥15%, concurrently attaining Decay Resistance Grade I (highest protection level).

ACKNOWLEDGMENTS

The authors are grateful for the support of the Jilin Province Science and Technology Development Project, Grant No. 20250201077GX. The authors also acknowledge the technical

support from the Microbial Processing Platform provided by the Jilin Provincial Engineering Research Center of Forestry Biotechnology.

REFERENCES

1. Borreguero, A.M., Valverde, J.L., Rodríguez, J.F., Barber, A.H., Cubillo, J.J., and Carmona, M., 2011: Synthesis and characterization of microcapsules containing Rubitherm® RT27 obtained by spray drying, Chemical Engineering Journal, 166(1): 384-390.
2. Cao, J., 2006: Current status of wood preservation technologies and research abroad, Scientia Silvae Sinicae 1(07): 120-126.
3. Chen, C., Cheng, X., Wang, L., and Xu, M., 2022: Study on the decay resistance of modified nano-composite wood preservatives, Forest Engineering 38(06): 61-68.
4. Choi, B.S, Song, J., Song, M., 2018: Core–shell engineering of Pd–Ag bimetallic catalysts for efficient hydrogen production from formic acid decomposition, ACS Catalysis, 9(2): 819-826.
5. Chuang, S., Xingxia M., Mingliang, J., 2023: In-situ growth of hexaconazole/ polydopamine/hexadecyltrimethoxysilane in multi-scale structured wood to prepare superhydrophobic wooden materials with decay resistance, Chemical Engineering Journal, 476, 146396.
6. Cui, Y., Zhao, Y., Tian, Y., Zhang, W., Lü, X., and Jiang, X., 2012: The molecular mechanism of action of bactericidal gold nanoparticles on *Escherichia coli*, Biomaterials 33(7): 2327-2333.
7. Rockwood, D.L., Winandy, J.E., & Gribbins, N.R., 2022: Processing and wood factors influence medium density fiberboard production from young *Eucalyptus grandis, eamplifolia, corymbia torelliana,* and cottonwood grown in Florida USA, Forests, 13(2): 266-278.
8. Emmerich, L., Bleckmann, M., Strohbusch, S., Brischke, C., Bollmus, S., 2021: Growth behavior of wood-destroying fungi in chemically modified wood: Wood degradation and translocation of nitrogen compounds, Holzforschung 75(9): 786-797.
9. Gao, F., Zhang, Y., You, H., Li, Z., Du, Y., 2021: Solvent-mediated shell dimension reconstruction of Core@ Shell PdAu@ Pd nanocrystals for robust C1 and C2 alcohol electrocatalysis, Small, 17(32): 2101428.
10. He, X.Y., Kong, F.X., Wang, Y.W., Shao, H.L., Bao, Y.J., Xu, L., and He, X.H.,2021: Study on wood properties and flooring application of domestic plantation teak, Forest Engineering 37 (04): 47-57.
11. Han, C.Y., Pang, J.Y., Sun, Y.X., 2023: Development of a functional wood anti-cracking agent based on EVA, Forest Engineering 39(06): 95-100+108.
12. Jiang, N.H., Zhao, H.L., and Liu, M., 2022: Drivers and potential of forest resource growth in China: Based on the Ninth National Forest Inventory, Journal of Forestry and Grassland Policy Research 2(03): 64-71.

13. Jin, G., Qin, H., Cao, H., Qian, S., Zhao, Y., Peng, X., and Chu, P.K., 2014: Synergistic effects of dual Zn/Ag ion implantation in osteogenic activity and antibacterial ability of titanium, Biomaterials 35(27):7699-7713.
14. Jiang, H., Xiong, Y. X., Li, H., 2025: Application of *Trichoderma virens* NY45 alone and in combination with copper azole for wood biopreservation. Journal of Forestry Engineering 11(01): 36-42.
15. Li, Y., Yang, Y., Qing, Y., Li, R., Tang, X., Guo, D., and Qin, Y., 2020: Enhancing ZnO-NP antibacterial and osteogenesis properties in orthopedic applications: A review, International Journal of Nanomedicine 15: 6247-6262.
16. Lei, W., Xiao, Z., Shi, R., 2023: Application of pH-responsive functionalized hollow mesoporous organosilica nanoparticles for wood preservation, Materials & Design, 225, 111538.
17. Lu, Z., Huang, Y., Chen, N., Liu, C., Wang, X., Ren, B., 2024: Self-reconstruction of core–shell structured electrocatalysts for tailoring reaction pathways revealed by electrochemical surface-enhanced Raman spectroscopy, ACS Catalysis, 14(8): 6204-6210.
18. Mohandas, A., Krishnan, A.G., Biswas, R., Menon, D., and Nair, M.B. ,2017: Antibacterial and cytocompatible nanotextured Ti surface incorporating silver via single step hydrothermal processing, Materials Science and Engineering: C 75:115-124.
19. Mo, Z., Jing, C., Zhao, W.,2023: Preparation of SiO_2@ EVA core-shell particles via post-emulsification method with polydisperse SiO_2 particle sizes and the critical thickness-to-diameter ratio in PA6/SiO_2@EVA system, Applied Surface Science, 2023,614, 156051.
20. Persaud, I., Raghavendra, A.J., Paruthi, A., Alsaleh, N.B., Minarchick, V.C., Roede, J.R., and Brown, J.M., 2020: Defect-induced electronic states amplify the cellular toxicity of ZnO nanoparticles, Nanotoxicology 14(2):145-161.
21. Selim, M.S., Shenashen, M. A., Elmarakbi, A., Fatthallah, N.A., Hasegawa, S.I., El-Safty, and S.A., 2017: Synthesis of ultrahydrophobic and thermally stable inorganic-organic nanocomposites for self-cleaning foul release coatings, Chemical Engineering Journal 320:653-666.
22. Sun, F.L., Kakwara, P.N., Wu, H.P., Qian, J.J., Yang, X.S., Rao, J., and Guo, M.,2017: Overview of bamboo and wood preservation technologies, Journal of Forestry Engineering 2(05): 1-8.
23. Shams, S., Khan, A.U., Yuan, Q., Ahmad, W., Wei, Y., Khan, Z.U.H., and Ullah, S., 2019: Facile and eco-benign synthesis of Au@ Fe_2O_3 nanocomposite: efficient photocatalytic, antibacterial and antioxidant agent, Journal of Photochemistry and Photobiology B: Biology 199, article 111632.
24. Teng, T.J., Arip, M.M., Sudesh, K., Nemoikina, A., Jalaludin, Z., Ng, E.P., Lee, H.L., 2018: Conventional technology and nanotechnology in wood preservation: A review, BioResources 13(4):9220-9252.
25. Xi, L.X., and Jiang, M.L., 2013: Advances in triazole wood preservatives, China Forest Products Industry 40(04):3-8.
26. Yang, X.M., 2011: Application status and environmental/health assessment of CCA, Journal of Sichuan Forestry Science and Technology 32(01):69-73.

27. Zhang, J.B., Huang, H.B., Zhang, C.W., and Guo, M.H., 2016: Research status and prospects of biomass wood preservatives, New Chemical Materials 44(04): 35-37+40.
28. Zhao, J.X., Zhang, B.P., Li, Y., Yan, L.P., and Wang, S.J., 2012: Optical and photocatalytic properties of TiO_2/Ag–SiO_2 nanocomposite thin films, Journal of Alloys and Compounds 535: 21-26.
29. Zhang, Q., Lv, L., Zhou, Y. F., 2025: Study on the antimicrobial properties of wood modified with silver-loaded nano-TiO_2 against common fungal species, Forestry Science and Technology 50(02): 70-74.

TING LIU, YAOXING SUN*, HONGGANG ZHAO*, HUACHUN QI, JIUYIN PANG
BEIHUA UNIVERSITY
SCHOOL OF MATERIALS SCIENCE AND ENGINEERING
132013 JILIN, CHINA
*Corresponding authors: sunyaoxing@sina.com; mailzhaoyang@163.com